Remote Sensing of Environment 253 (2021) 112222

Contents lists available at ScienceDirect

Remote Sensing of Environment

journal homepage: www.elsevier.com/locate/rse

Assimilation of SMAP and ASCAT soil moisture retrievals into the JULES land surface model using the Local Ensemble Transform Kalman Filter

Eunkyo Seo [a,1], Myong-In Lee [a,*], Rolf H. Reichle [b]

[a] School of Urban and Environmental Engineering, Ulsan National Institute of Science and Technology, Ulsan, Republic of Korea
[b] Global Modeling and Assimilation Office, NASA Goddard Spaceflight Center, Greenbelt, MD, United States

ARTICLE INFO

Keywords:
Soil moisture assimilation
LETKF
JULES LSM
SMAP
ASCAT

ABSTRACT

A land data assimilation system is developed to merge satellite soil moisture retrievals into the Joint U.K. Land Environment Simulator (JULES) land surface model (LSM) using the Local Ensemble Transform Kalman Filter (LETKF). The system assimilates microwave soil moisture retrievals from the Soil Moisture Active Passive (SMAP) radiometer and the Advanced Scatterometer (ASCAT) after bias correction based on cumulative distribution function fitting. The soil moisture assimilation estimates are evaluated with ground-based soil moisture measurements over the continental U.S. for five consecutive warm seasons (May–September of 2015–2019). The result shows that both SMAP and ASCAT retrievals improve the accuracy of soil moisture estimates. Especially, the SMAP single-sensor assimilation experiment shows the best performance with the increase of temporal anomaly correlation by $\Delta R \sim 0.05$ for surface soil moisture and $\Delta R \sim 0.03$ for root-zone soil moisture compared with the LSM simulation without satellite data assimilation. SMAP assimilation is more skillful than ASCAT assimilation primarily because of the greater skill of the assimilated SMAP retrievals compared to the ASCAT retrievals. The skill improvement also depends significantly on the region; the higher skill improvement in the western U.S. compared to the eastern U.S. is explained by the Kalman gain in the two experiments. Additionally, the regional skill differences in the single-sensor assimilation experiments are attributed to the number of assimilated observations. Finally, the soil moisture assimilation estimates provide more realistic land surface information than model-only simulations for the 2015 and the 2016 western U.S. droughts, suggesting the advantage of using satellite soil moisture retrievals in the current drought monitoring system.

1. Introduction

Land surface conditions play an important role in drought development, runoff generation, and many other processes related to the land-atmosphere exchange of energy and water (Bateni and Entekhabi, 2012; Seneviratne et al., 2010; Seneviratne et al., 2006). In particular, soil moisture states have a memory operating at 1–2 month (i.e., sub-seasonal) time scales (Koster et al., 2011; Seo et al., 2019; Seo et al., 2020). In future climate scenarios, the role of the land surface may increase with enhanced land-atmosphere coupling, and an expansion of the coupling area may increase the potential risk of severe droughts and heat waves (Dirmeyer et al., 2013). Soil moisture conditions are typically inferred from (1) ground-based observations, (2) remote-sensing retrievals from active and passive microwave satellite sensors, or (3) land surface model (LSM) simulations forced with surface meteorological data from observations or atmospheric analysis estimates. In situ measurements provide the most reliable land information of the surface and sub-subsurface layers at the measurement location but have limitations in terms of spatial and temporal resolution and coverage. Satellite remote sensing provides only surface soil moisture conditions due to the limitation in penetration depth. LSM simulations provide complete spatio-temporal coverage but contain potentially large uncertainties in the model physical parameterization and the surface meteorological forcing variables.

Space-borne microwave instruments can be used to retrieve surface soil moisture by measuring soil dielectric properties. Past and current microwave instruments include the X-band (10.7 GHz) and C-band (6.9 GHz) channels of the passive Advanced Microwave Scanning

* Corresponding author at: School of Urban and Environmental Engineering, Ulsan National Institute of Science and Technology, 50 UNIST-gil, Ulsan 44919, Republic of Korea.
E-mail address: milee@unist.ac.kr (M.-I. Lee).
[1] Current address: Center for Ocean-Land-Atmosphere Studies, George Mason University, Fairfax, VA, United States.

https://doi.org/10.1016/j.rse.2020.112222
Received 23 June 2020; Received in revised form 23 November 2020; Accepted 24 November 2020
Available online 9 December 2020

Radiometer (AMSR-E; Owe et al., 2008; Owe et al., 2001) and its successor (AMSR2; Parinussa et al., 2015), the X-band (10.65 GHz) passive Tropical Rainfall Measuring Mission (TRMM) Microwave Imager (TMI; Gao et al., 2006), the C-band (6.63 GHz) passive Scanning Multichannel Microwave Radiometer (SMMR; De Jeu, 2003), the C-band (~5.4 GHz) multi-angular Sentinel-1 Synthetic Aperture Radar (SAR) data (Torres et al., 2012), and the C-band (5.3 GHz) active (radar) microwave Advanced Scatterometer (ASCAT; Wagner et al., 2013). The Soil Moisture and Ocean Salinity (SMOS; Kerr et al., 2010) and Soil Moisture Active Passive (SMAP; Entekhabi et al., 2010a) sensors measure passive microwaves at L-band (1.4 GHz) frequencies and are specifically designed to retrieve surface soil moisture. The typical soil penetration depth ranges from ~1–2 cm for X- and C-band retrievals to ~5 cm for L-band retrievals. The spatial (horizontal) resolution is ~20 km for X- and C-band retrievals and ~ 40 km for L-band retrievals.

Land data assimilation can be used to combine the soil moisture information from diverse satellite observations with the advantages of LSMs (Reichle, 2008). Most previous studies on land data assimilation adopted simplified or ensemble-based filtering methods such as the Extended Kalman Filter (EKF) or the Ensemble Kalman Filter (EnKF) rather than variational assimilation approaches, which require an adjoint of the land surface model that is difficult to derive (Lahoz and De Lannoy, 2014; Reichle et al., 2001). In ensemble-based methods, the background error covariance is diagnosed from the ensemble of (nonlinear) land model simulations. The NASA Goddard Earth Observing System (GEOS) land data assimilation system adopted the EnKF to constrain modeled land surface variables using satellite measurements such as soil moisture (Reichle et al., 2008; Reichle et al., 2002a; Reichle et al., 2002b), land surface temperature (Reichle et al., 2010), snow (De Lannoy et al., 2010), and terrestrial water storage (Forman et al., 2012). The European Centre for Medium-Range Weather Forecasts numerical weather prediction system relies on an EKF-based land surface data assimilation system that combines conventional near-surface observations (two-meter air temperature and relative humidity) with ASCAT surface soil moisture retrievals (Albergel et al., 2012; De Rosnay et al., 2013).

Several previous studies perform soil moisture assimilation experiments and evaluate the resulting soil moisture estimates against in situ observations. For example, Liu et al., (2011) demonstrated that assimilating AMSR-E soil moisture retrievals increases soil moisture skill compared to an LSM simulation without data assimilation (often referred to as the "open loop") and Albergel et al., (2012) showed a benefit of assimilating ASCAT satellite for improved soil moisture analysis. Assimilating ASCAT and AMSR-E soil moisture retrievals yields comparable skill improvements, and assimilating both data sets consistently matched or exceeded the best results from the single-sensor assimilation experiments (Draper et al., 2012). De Lannoy and Reichle (2016) found that the assimilation of SMOS soil moisture retrievals or brightness temperatures results in improved soil moisture estimates over North America and Ridler et al. (2014) also addressed the improvement in Western Denmark. Moreover, Pan et al. (2016) suggested that SMAP provides significant added value for data assimilation. Similarly, Lievens et al. (2017) demonstrated soil moisture skill improvements through SMAP and Sentinel-1 data assimilation. Finally, the global SMAP Level-4 Surface and Root-zone Soil Moisture (L4_SM) product, which has been produced operationally by assimilating SMAP L-band brightness temperature observations into the NASA Catchment LSM at 9-km resolution with ~3-day latency since 2015 (Reichle et al., 2017a; Reichle et al., 2017b), has significantly higher skill than model-only soil moisture estimates (Reichle et al., 2019).

Based on the aforementioned studies, SMAP satellite retrievals have a strong sensitivity to soil moisture in a slightly deeper surface layer and perform better in satellite data assimilation than other satellite soil moisture retrievals (Al-Yaari et al., 2019). On the other hand, ASCAT satellite retrievals have been available from the Meteorological Operational Satellite (METOP)-A launched in 2006, the METOP-B in 2012, and the most recently launched METOP-C in 2018, which provide the data with wide spatial coverage for global analysis as well as long-term data useful for climate reanalysis. Due to these advantages, SMAP and ASCAT have been widely used by many U.S. and European institutes in operation and research for the satellite soil moisture data assimilation. One of the motivations of this study is to evaluate the skill improvement of soil moisture estimates through the assimilation of these two widely-used satellite retrievals, which are produced by different remote sensing technologies in terms of radiation bands and active or passive sensors. A careful comparison of the data from the observation data sensitivity experiments using identical LSM and the data assimilation technique will help understand the relative advantages or disadvantages of the two satellite retrievals. Another motivation of this study is to apply several metrics that measure the skill improvement in the satellite soil moisture data assimilation in a quantitative manner. The skill improvement can be contributed by many factors, such as the quality of the assimilated satellite retrievals (relative to the open loop estimates), the number of remote-sensing data being assimilated, and the accuracy of the model background. Often these impacts are entangled in the data assimilation system output and hardly decomposed by conventional metrics. In this regard, there are insufficient studies in previous literature that quantify the individual contribution of each factor to the skill increase. One goal of this study is to help identify the dominant factors. This information can eventually be utilized for planning future soil moisture remote sensing technologies.

In this study, we carry out a series of soil moisture data assimilation experiments with active and passive microwave retrievals designed to investigate the impact based on the following objectives. The first objective is to investigate the skill improvement of surface and root-zone soil moisture through the assimilation of SMAP and ASCAT soil moisture retrievals into the Joint U.K. Land Environment Simulator (JULES) LSM using the Local Ensemble Transform Kalman Filter (LETKF), a variant of the EnKF. Key distinguishing features of the LETKF are its efficiency of parallel computation through separating the domain into independent local patches and that the LETKF enables to inflate the analysis error covariance. Skill improvement relative to model-only (open loop) estimates is assessed versus in situ soil moisture measurements. The second objective is to introduce assimilation metrics that break down the skill improvement into three quantitative components: (i) the skill of the assimilated soil moisture retrievals relative to open loop simulation, (ii) an approximation of the Kalman gain, and (iii) the number of assimilated observations. Finally, following previous studies that demonstrated the value of satellite soil moisture assimilation to enhance the drought monitoring (Mladenova et al., 2019; Xu et al., 2020), we assess the benefit of assimilating satellite soil moisture retrievals in the context of drought monitoring, specifically its potential for the U.S. drought monitoring system (https://droughtmonitor.unl.edu/).

The paper is organized as follows. Section 2 introduces the model and datasets used in this study. Section 3 describes the assimilation methodology, our validation approach, and the assimilation metrics. Section 4 presents and discusses the results of this study. Finally, Section 5 summarizes the results and their implications for future studies.

2. Model and data

2.1. JULES land surface model

This study uses the JULES community LSM (Best et al., 2011) developed by the U. K. Met Office. The soil moisture sub-model consists of 4 vertical layers of 0.1, 0.25, 0.65, and 2 m in thickness. In this study, the model is set up with a 50 km spatial resolution. Land cover classes in JULES consist of five plant functional types (broadleaf trees, needleleaf trees, C3 temperate grass, C4 tropical grass, and shrubs) and four non-vegetation types (urban, inland water, bare soil, and land-ice). Surface parameters (e.g., albedo, roughness length) are specified for each land cover, and the model prognostic variables (e.g., soil moisture) are

Table 1
Parameters for perturbations to near-surface atmospheric boundary forcing variables and JULES soil moisture model prognostic variable at 0–10 cm (top) layer.

Perturbation variables	Additive (A)/ Multiplicative (M)	Standard deviation	AR1 correlation time scale	Spatial correlation
Precipitation	M	0.5	1 day	50 km
Downward shortwave (SW)	M	0.3	1 day	50 km
Downward longwave (LW)	A	50 W m^{-2}	1 day	50 km
Soil moisture content	A	0.002 m^3 m^{-3}	3 h	50 km

A first-order auto-regressive (AR1) model is used for temporal correlations. Spatial correlation lengths scales are isotropic.

determined in response to atmospheric forcing variables, including 2-m air temperature and humidity, precipitation, 10-m wind speed, radiative fluxes, and pressure at the surface. In this study, the surface meteorological forcing variables except precipitation are obtained from the 6-hourly, 55-year Japanese Reanalysis (JRA-55) with 0.56° spatial resolution (Kobayashi et al., 2015). The forcing dataset is linearly interpolated to the model spatial resolution. Precipitation forcing, which is the most critical input determining soil moisture accuracy in land surface modeling, uses the Global Satellite Mapping of Precipitation (GSMaP; Aonashi et al., 2009; Kubota et al., 2007; Ushio et al., 2003; Ushio et al., 2009). GSMaP originally provides an hourly, gauge-calibrated rain rate with a 10 km spatial resolution over a quasi-global domain (60°S–60°N). This study uses the GSMaP precipitation data within the 60°S–60°N latitude band and JRA-55 for the rest of the model domain. GSMaP has been processed to the 6-hourly averaged data to match the temporal resolution of the JRA-55 reanalysis.

Errors in the JULES model estimates are propagated through an ensemble approach. Following Reichle et al., (2008), selected surface meteorological forcing variables and model prognostic variables are perturbed with random numbers, specifically radiation, rainfall, and soil moisture. As displayed in Table 1, normally distributed, additive perturbations are used for the 0–10 cm (top) layer soil moisture prognostic variable and the longwave radiation forcing, while lognormally distributed multiplicative perturbation are used for the precipitation and shortwave radiation forcing. The ensemble mean of additive and multiplicative perturbations is 0 and 1, respectively. All random perturbations are subject to a first-order autoregressive (AR1) process with correlation time scales of 1 day for forcing variables and 3 h for soil moisture content. Moreover, perturbations are also correlated spatially with a correlation scale of 50 km following an isotropic exponential decay model. In addition, cross-correlations, imposed on perturbations of the precipitation and radiation fields, ensure physical consistency between the meteorological forcing variables. For example, a positive perturbation of the downward shortwave radiation is (statistically) paired with a negative perturbation of the downward longwave radiation and precipitation. A detailed description of perturbing the surface meteorological forcing and model prognostic variables is provided in Reichle et al., (2008).

2.2. Data

2.2.1. In situ soil moisture measurements

For the validation, this study uses in situ soil moisture measurements from the U.S. Natural Resources Conservation Service (NRCS) Soil Climate Analysis Network (SCAN; Schaefer et al., 2007), the U.S. Climate Reference Network (USCRN; Diamond et al., 2013; Bell et al., 2013), and the Snowpack Telemetry (SNOTEL) network. Data are provided as hourly measurements at 5, 10, and 20 cm depths with flags for problematic observations in terms of data quality. Only datasets of "good" quality and simultaneously measured at three different depths are used. We further discard unrealistic values such as the data beyond the physically possible range and exclude measurements when the soil is frozen. After the quality control of the hourly data, we calculate daily mean soil moisture.

Two additional screens are imposed before a measurement site is used in the validation of the assimilation estimates. First, sites must have the data available more than 50% during the entire validation period. Second, sites with the particularly poor skill of either the SMAP or ASCAT satellite retrievals relative to the open loop estimates ($R_{sat} - R_{openloop} < -0.2$) are excluded. This criterion screens out 109 in situ measurement stations out of 244, and the remaining 135 stations are used for the validation. This second screen avoids validation at sites where the satellite data should not be assimilated in the first place, leaving the enhancement of the QC algorithm for future work. The network sites used in the validation of the data assimilation results are mapped in Fig. 1. Finally, in situ "surface" soil moisture corresponds to measurements at 5 cm depth, and in situ "root-zone" soil moisture corresponds to a layer thickness-weighted average of the measurements at 5, 10, and 20 cm depths.

Validation results are broken down by land cover type (Fig. 1). Land

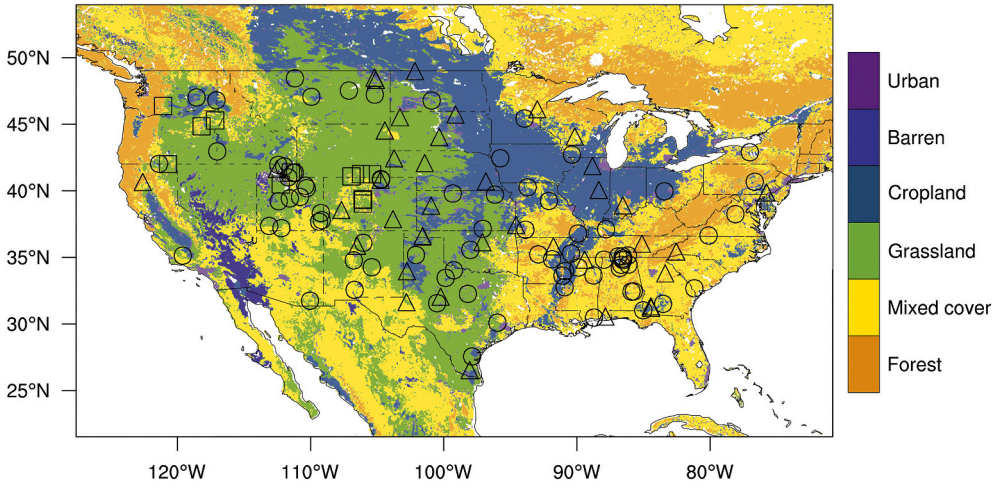

Fig. 1. Location of monitoring sites of the SCAN (circle), USCRN (triangle), and SNOTEL (square) networks over the continental U.S. Overlaid are the MODIS land cover classes with "forest" consisting of IGBP classes 1–5 and "mixed cover" consisting of IGBP classes 6–9 and 14.

cover is from the MODIS Collection 5 product (Friedl et al., 2010), which provides data at 500 m spatial resolution with 17 International Geosphere-Biosphere Programme (IGBP) classifications (Loveland and Belward, 1997): (1) evergreen needleleaf forests, (2) evergreen broadleaf forests, (3) deciduous broadleaf forests, (4) deciduous needleleaf forests, (5) mixed forests, (6) closed shrubland, (7) open shrublands, (8) woody savannas, (9) savannas, (10) grasslands, (11) permanent wetlands, (12) croplands, (13) urban and built-up lands, (14) cropland/natural vegetation mosaics, (15) permanent snow and ice, (16) barren, and (17) water. For the analysis by land cover, we grouped IGBP classes 6–9 and 14 into a broader "mixed land cover" class. The validation is performed at the point of in situ observations in which 0.5 deg. modeled soil moisture estimates are interpolated. If the point of in situ sites is on a specified land cover, we define the result over there.

2.2.2. Assimilated satellite soil moisture retrievals

This study assimilates near-surface soil moisture datasets provided by the L-band (1.4 GHz) passive (radiometer) microwave SMAP Level-2 product (O'Neill et al., 2019) and the C-band (5.3 GHz) active (radar) microwave ASCAT product (https://navigator.eumetsat.int/product/EO:EUM:DAT:METOP:SOMO25). The SMAP and ASCAT data are available from May 2015 and from October 2006 to the present, respectively. As mentioned above, the spatial resolution and soil penetration depth differ for the two datasets. Moreover, the SMAP retrievals, unlike the ASCAT retrievals, are subject to errors in their ancillary inputs of soil temperature and vegetation water content (Paloscia and Pampaloni, 1988; Schmugge et al., 1986). In contrast, the ASCAT data are more sensitive to noise from multiple scattering, especially over topographically complex, wetland, and forest regimes (Dobson and Ulaby, 1986).

The observation error standard deviations in the data assimilation are set to 0.04 $m^3\ m^{-3}$ for SMAP retrievals (Chan et al., 2016) and 10% (in relative saturation units) for ASCAT retrievals (Dorigo et al., 2010). In both cases, spatially and temporally constant values are used. Prior to assimilation, quality control for the satellite data is applied based on the data quality flags provided with each satellite dataset. Additionally, observations are discarded where MODIS land cover indicates forests (> 60% trees and woody vegetation) or grid cells with a wetland cover area fraction greater than 10% (indicated by ASCAT data). The ASCAT data are also discarded, where topographical complexity exceeds 10% (Draper et al., 2012). Finally, we exclude soil moisture retrievals from the assimilation whenever the modeled surface temperature is less than 274 K, precipitation exceeds 50 mm day^{-1}, or the land is covered by snow in the model simulation.

3. Methodology

3.1. Data assimilation method

The assimilation is performed using the LETKF (Hunt et al., 2007; Miyoshi and Yamane, 2007). Similar to the EnKF used in the SMAP L4_SM algorithm (Reichle et al., 2017b), the LETKF scheme used here separates the domain into a number of independently processed local patches. When analyzing the model states at the center of each local patch, all nearby observations within the local patch are used, which allows for efficient parallel computations in a spatially distributed analysis. Unlike the EnKF of the L4_SM algorithm, the LETKF used here is a deterministic filter that does not perturb the assimilated observations, thereby avoiding the concomitant sampling noise.

In the following, X denotes the state vector within a specified local patch, and subscripts b and a denote the prior (i.e., background) and the updated (i.e., analysis) states, respectively. The dimension of X is $L \times N$ composed of an L dimensional local patch of N ensemble members. Generally, the local patch could be 3-dimensional, characterized by horizontal and vertical grid extent. However, this study defines only a 2-dimensional, horizontal local patch (150 km × 150 km) because only top layer soil moisture is analyzed. Formally, the analyzed state vector X_a is given by

$$X_a = \overline{X}_a + \delta X_a \tag{1}$$

where $\overline{X}_a$ is an $L \times 1$ matrix of analysis ensemble means and δX_a denotes an $L \times N$ matrix of analysis perturbations. They are defined by

$$\overline{X}_a = \overline{x}_b + \delta\tilde{x}_a \tag{2}$$

$$\delta\tilde{x}_a = \delta X_b \tilde{P}_a (\delta Y)^T R^{-1} d \tag{3}$$

In Eq. (2), $\overline{x}_b$ indicates the background forecast mean and $\delta\tilde{x}_a$ denotes the analysis increment. In Eq. (3), δX_b, $\tilde{P}_a$, δY, R, and d are background forecast perturbation, analysis error covariance, forward operated forecast ensemble perturbations, observation error covariance, and observational innovation, respectively. The observational innovation vector d is the difference between observations y_0 and their background ensemble mean counterparts $\overline{H(X_b)}$, where H is possibly a nonlinear observation operator and is replaced with the linearized version. The observation operator projects the modeled soil moisture background to the locations of the satellite observations using bilinear interpolation.

The forward-operated background forecast ensemble and the analysis error covariance in observation space are written as

$$\delta Y = H(X_b) \tag{4}$$

$$\tilde{P}_a = \left[\delta Y^T R^{-1} \delta Y + (N-1) I/\rho\right]^{-1} \tag{5}$$

where ρ is a covariance inflation parameter for the analysis error covariance. The parameter ρ helps avoid the underestimation of the covariance which is a common problem of filter divergence caused by the assumption of spatially and temporally constant forcing and observation errors and the use of a limited number of ensemble members. In this study, we apply a multiplicative covariance inflation of 20% of the spread (i.e., ρ =1.2). After calculating analysis ensemble states for all independent local patches, we collect the analysis results from each local patch into analysis for the entire domain.

Covariance localization is a useful method to moderate spurious sample error correlation estimates by applying a distance-dependent reduction of the sample error covariance estimates (Hamill et al., 2001; Houtekamer and Mitchell, 2001). The LETKF scheme contains the weighting function of the localization by separation into local patches. The function weights 1 inside and 0 outside the local patch and by weighting the observational error covariance according to the distance from the local patch center (Hunt et al., 2007). The covariance localization via the weighting function within the local patch works by assigning larger errors to more distant observations (Miyoshi and Yamane, 2007). The more closely the weighting function of the covariance localization is centered around the local patch center, the more the scheme resembles a 1-D filter. It can be realized by multiplying the observation error covariance by the inverse of the smooth weighting function within each local patch in which the range of weighting function is possibly 0 to 1. The weighting function $w(r_i)$ is based on a Gaussian function as

$$w(r_i) = exp\left(-r_i^2/2\sigma^2\right) \tag{6}$$

where r_i denotes the distance of i-th observation within each local patch from the local patch center and σ represents a localization scale parameter. In this experiment, we use a localization length scale parameter value of 30 km. That is, the LETKF is set up almost like a 1-D filter, with weights of just 10^{-2}– 10^{-3} near the edge of the local patch.

3.2. Bias correction

There is often a large discrepancy between soil moisture contents from remote sensing retrievals and LSMs, owing to uncertainties in

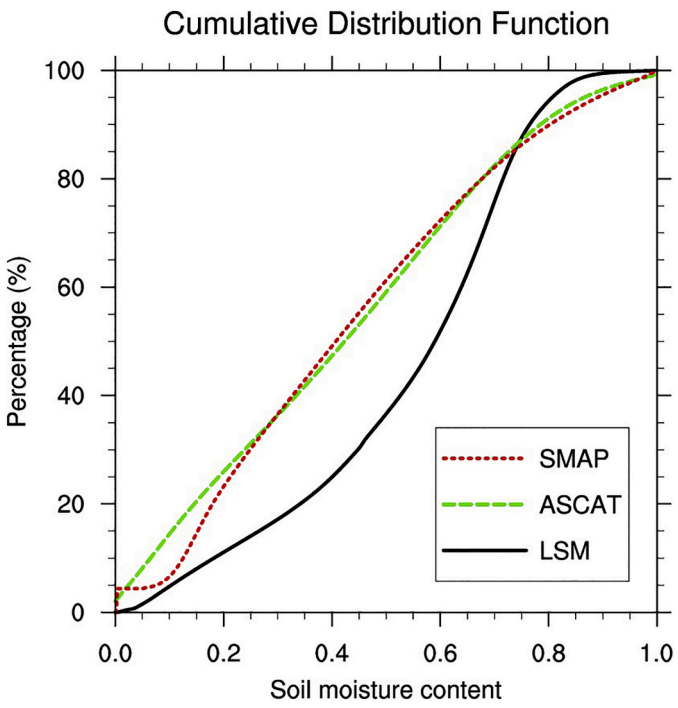

Fig. 2. The cumulative distribution function of surface soil moisture content as a fraction of saturation from SMAP retrievals (April 2015–December 2019), ASCAT retrievals (January 2010–December 2019), and the LSM open loop simulation (January 2010–December 2019) over North America (130°W–75°W, 30°N–50°N).

model physics and forcing data and differences in the associated layer depths. These discrepancies manifest in sometimes large biases in the mean, variance, and higher-moment statistics of soil moisture between the satellite retrievals and the model simulation. One way to correct for such biases is to match the cumulative distribution functions (CDFs) between the satellite dataset and the model simulation (Reichle and Koster, 2004). Such a CDF matching adjusts all moments and differs from a linear rescaling that matches only the mean values and standard deviations based on the assumption of a Gaussian distribution (Yilmaz and Crow, 2013). CDF matching, which is used here, is thus more appropriate for representing skewed datasets and also avoids violating the variables' physical bounds. Over North America, for instance, the CDFs of surface soil moisture from SMAP retrievals, ASCAT retrievals, and the LSM open loop simulation differ considerably (Fig. 2). Prior to data assimilation, the raw SMAP and ASCAT soil moisture retrievals are rescaled to the LSM climatology based on the CDFs, which is done separately for each grid cell. The specified observation error standard deviation is also rescaled using the ratio of the standard deviation of the satellite to modeled soil moisture time series at each grid cell (Liu et al., 2011).

3.3. Data assimilation experiments

This study performs three data assimilation experiments by specifying different sets of soil moisture retrieval data to be assimilated into the JULES LSM, including two single-sensor experiments using SMAP and ASCAT satellite retrievals, respectively, and a combined SMAP plus ASCAT multi-sensor experiment, hereafter referred to as DA(SMAP), DA (ASCAT), and DA(SMAP+ASCAT), respectively. The specific description of the LSM configuration and data assimilation method was provided in Sections 2.1 and 3.1, respectively. The experiments use 12 ensemble member and a 3-h assimilation cycle. They are conducted for May–September of 2015–2019. As a baseline, a 12-member, open loop ensemble experiment is also performed using the same ensemble perturbations but no data assimilation. The open loop skill serves as a baseline for measuring the skill improvement from the satellite data assimilation.

3.4. Validation strategy

The assimilation and open loop estimates are validated against the in situ soil moisture measurements described in Section 2.2.1. This study primarily measures the skill in temporal variations using the Pearson correlation coefficient (R) applied to anomaly time series, calculated by removing monthly-mean values for each calendar month. This anomaly correlation is computed for daily averages of the surface and root-zone anomaly soil moisture. This study also measures the data assimilation performance based on the unbiased root-mean-square error (ubRMSE) of the raw soil moisture time series (Entekhabi et al., 2010b), which avoids some of the shortcomings of the RMSE metric in the presence of mean bias. Based on the Fisher Z transform, we compute approximate 95% confidence levels for the anomaly correlations at in situ sites. These confidence levels depend on the estimated R value and the number of degrees of freedom. The 95% confidence intervals are calculated by averaging the 95% confidence intervals across the in situ sites and subsequently dividing by the square root of the number of sites. The model surface soil moisture is validated against in situ measurements at 5 cm depth, and the model root-zone soil moisture is validated against the depth-weighted root-zone in situ measurements defined in Section 2.2.1. The skill improvement of the data assimilation with respect to the open loop is defined as the R value of the assimilated product minus that of the open loop model.

3.5. Assimilation metrics

This study introduces quantitative assimilation metrics to decompose skill improvement from data assimilation. Three components determine the impact of the data assimilation on the model estimates: (1) the skill difference between the satellite retrievals and the open loop estimates (ΔR_{sat}), (2) the approximate weighting of the assimilated observations in the analysis update (KG), and (3) the average number of assimilated observation samples (N_{sat}). Each metric is written as

$$\Delta R_{sat} = R_{sat} - R_{openloop} \tag{7}$$

$$KG = \sum_{t=1}^{N_{days}} \left[\frac{E_b(t)}{E_b(t) + E_o(t)} \right] \Big/ N_{days} \tag{8}$$

$$N_{sat} = \sum_{t=1}^{N_{days}} \sum_{i=1}^{n} w(r_i)_t \Big/ N_{days} \tag{9}$$

In Eq. (7), R_{sat} is the temporal anomaly correlation (Section 3.4) between remotely sensed retrievals (y_0) and the in situ surface soil moisture observations. Similarly, $R_{openloop}$ is the temporal anomaly correlation between the open loop surface soil moisture and the in situ measurements. In Eq. (8), $E_b(t)$ and $E_o(t)$ are the error variances of the model background and the observation of surface soil moisture at each analysis time, respectively, and N_{days} denotes the number of days over the entire assimilation period. By construction, the value of KG is bounded between 0 and 1. High values of KG imply that the analysis of soil moisture is closer to the observation than to the background. Note that KG is a rough approximation of the diagonal element of the Kalman gain matrix in the LETKF scheme. In Eq. (9), the number of assimilated observation samples is defined as the time average of the sum of the localization weights (i.e., Eq. (6)) within the local patch at each analysis time.

3.6. Soil moisture condition index

This study also applies the assimilated soil moisture information to

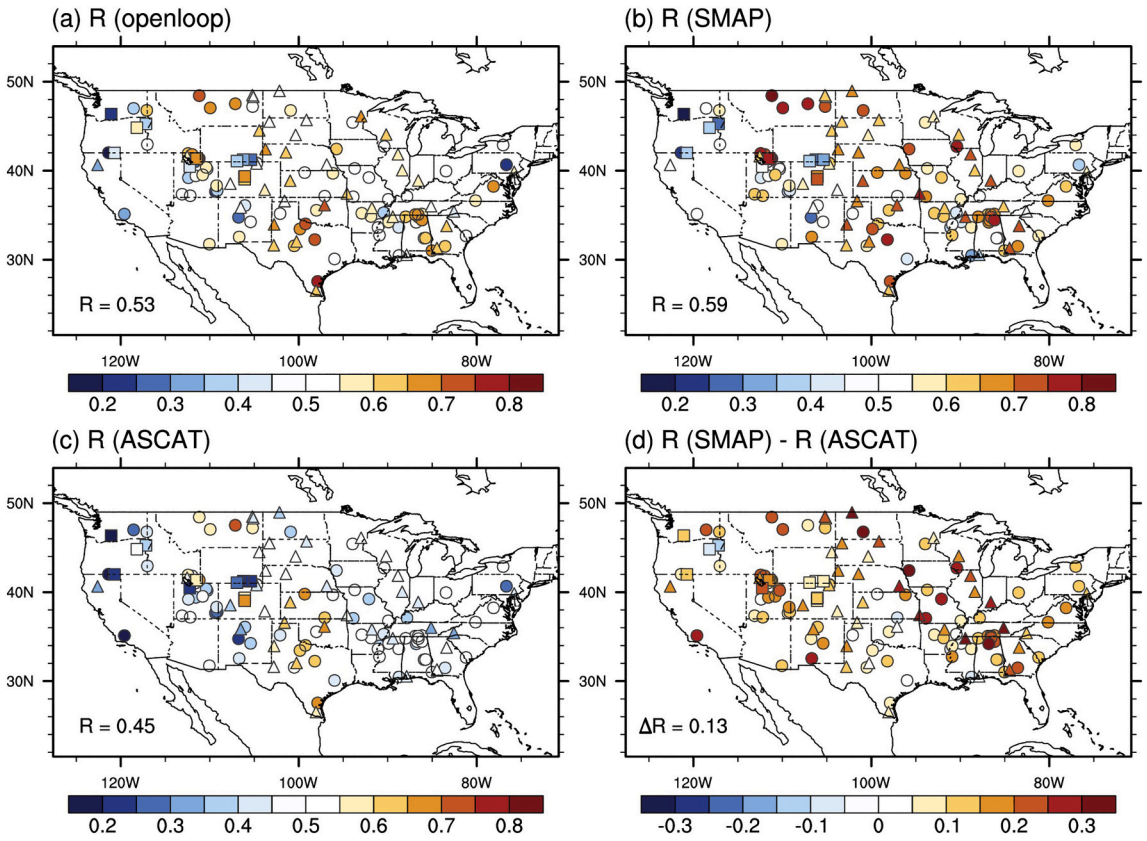

Fig. 3. Surface soil moisture skill measured as the anomaly correlation coefficient R with the in situ measurements from (a) the open loop model, (b) SMAP retrievals, and (c) ASCAT retrievals. (d) shows the skill difference between SMAP and ASCAT retrievals, with red (blue) colors indicating that SMAP retrievals have higher (lower) skill than ASCAT retrievals. (For interpretation of the references to colour in this figure legend, the reader is referred to the web version of this article.)

drought monitoring using the soil moisture condition index (SMCI) introduced in Zhang and Jia (2013). This index uses weekly-mean values and is designed to capture the development of short-term dryness. The index should be comparable across regions, regardless of the background climatology, and does not reflect seasonality. It is written as

$$SMCI = \frac{SM - SM_{min}}{SM_{max} - SM_{min}} \tag{10}$$

where SM represents a weekly-averaged surface soil moisture, and the

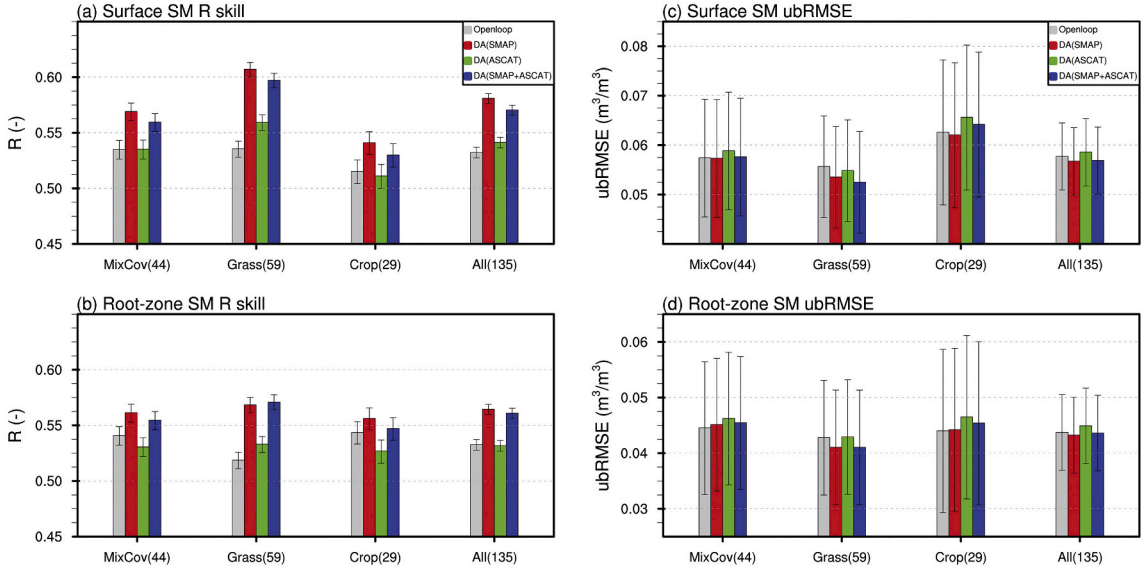

Fig. 4. (a, b) R skill and (c, d) ubRMSE of (a, c) surface and (b, d) root-zone soil moisture estimates from the open loop (gray), DA(SMAP) (red), DA(ASCAT) (green), and DA(SMAP+ASCAT) (blue). The soil moisture estimates are validated against in situ measurements over North America (see Fig. 1 for locations) and averaged for each land cover class. Error bars represent 95% confidence intervals. (For interpretation of the references to color in this figure legend, the reader is referred to the web version of this article.)

subscripts *max* and *min* indicate the maximum and the minimum values for each corresponding week at each grid cell from the 71 years (1948–2018) long-term JULES offline simulation. The first 62 years (1948–2009) of the LSM offline simulation are forced with surface meteorological data from Sheffield et al. (2006), and the rest of the period (2010–2018) is from the LSM run driven by the JRA-55 reanalysis corrected with the 6-hourly GSMaP rainfall. The index is bounded between 0 and 1. At a given grid cell, the closer the drought index is to zero, the more severe the drought.

4. Results

4.1. Skill of satellite and open loop soil moisture estimates

Before we investigate the results of the soil moisture assimilation, we examine the skill of the satellite and open loop estimates. Fig. 3 shows the anomaly correlation coefficient for the open loop (Fig. 3a), the SMAP retrievals (Fig. 3b), and the ASCAT retrievals (Fig. 3c) against in situ measurements in the continental U.S. The average R values of the open loop, SMAP retrievals, and ASCAT retrievals are 0.53, 0.59, and 0.45, respectively. The skill of SMAP is best overall and clearly better than that of ASCAT ($\Delta R \sim 0.13$) over the entire U.S. without any obvious regional pattern (Fig. 3d).

4.2. Skill of soil moisture estimates from data assimilation experiments

Fig. 4 compares the average skill of surface and root-zone soil moisture estimates from the open loop with the three experiments that assimilate (i) SMAP retrievals only, (ii) ASCAT retrievals only, and (iii) both SMAP and ASCAT retrievals. The average anomaly correlation skill of surface soil moisture (Fig. 4a) is increased in the assimilation experiments by 0.05 (DA(SMAP)), 0.01 (DA(ASCAT)), and 0.04 (DA (SMAP+ASCAT)), respectively, compared to the open loop ($R = 0.53$), which represents a statistically significant improvement (at the 5% significance level) when SMAP data are included in the assimilation. The relative performance is similar when measured with the ubRMSE, although the ubRMSE reductions are not statistically significant (Fig. 4c). The skill improvement is greater for grasslands than for the other land cover classes, which will be discussed further in the next subsection. The result implies that the satellite retrievals provide added value through data assimilation. Even though ASCAT observations are additionally assimilated in DA(SMAP+ASCAT) compared to DA(SMAP), the skill of DA(SMAP+ASCAT) is slightly worse than that of DA(SMAP), which suggests that the assimilation system is less optimal for DA (SMAP+ASCAT) than for DA(SMAP). Some sub-optimality is unavoidable because the satellite observations are assimilated into a non-linear model (here, JULES LSM) and the errors are never entirely Gaussian and uncorrelated. This suggests that there is little added benefit from assimilating the ASCAT retrievals, which have relatively poor skill compared to the SMAP retrievals and the open loop run (Fig. 3).

Although only surface soil moisture observations are assimilated, there is also an indirect positive impact on sub-surface (root-zone) soil moisture (Fig. 4b). The anomaly correlation of root-zone soil moisture is increased in the assimilation experiments by 0.04 (DA(SMAP) and DA (SMAP+ASCAT)), compared to the open loop (R = 0.53), but the skill improvements in the root-zone are not as large as those in the surface. In particular, the assimilation of SMAP retrievals results in a significant improvement of the root-zone soil moisture skill (except for crops), while the impact of the ASCAT assimilation on the root-zone skill is neutral on average. The neutral impact of the ASCAT assimilation on the root-zone soil moisture skill is expected because only the surface soil moisture states are updated directly in our analysis and the skill improvement in the surface soil moisture in DA(ASCAT) is marginal (Fig. 4a). The relative performance is again similar when measured with the ubRMSE, although the ubRMSE reductions are again not statistically significant (Fig. 4d). Finally, we obtained similar results for the surface

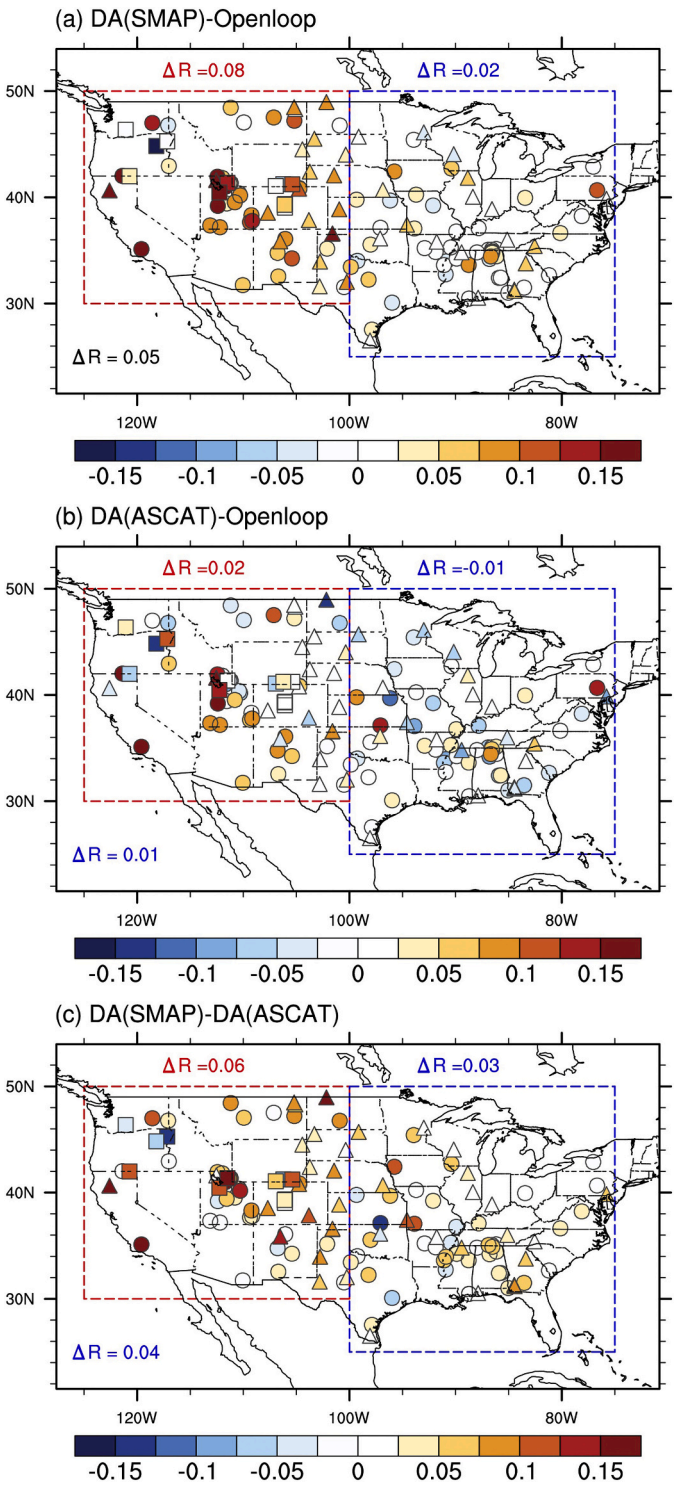

Fig. 5. Skill difference between surface soil moisture estimates from (a) DA (SMAP) and the open loop, (b) DA(ASCAT) and the open loop, and (c) DA (SMAP) and DA(ASCAT). The bottom-left value in each panel is averaged across the entire domain. The red and blue dashed boxes indicate the western and eastern U.S., respectively, and the value above the box represents the average of the values in each box. (For interpretation of the references to colour in this figure legend, the reader is referred to the web version of this article.)

and root-zone validation when using only days and locations for which satellite observations were assimilated (not shown).

The skill of soil moisture estimates from all assimilation experiments is commonly increased, but the magnitude of the improvements depends

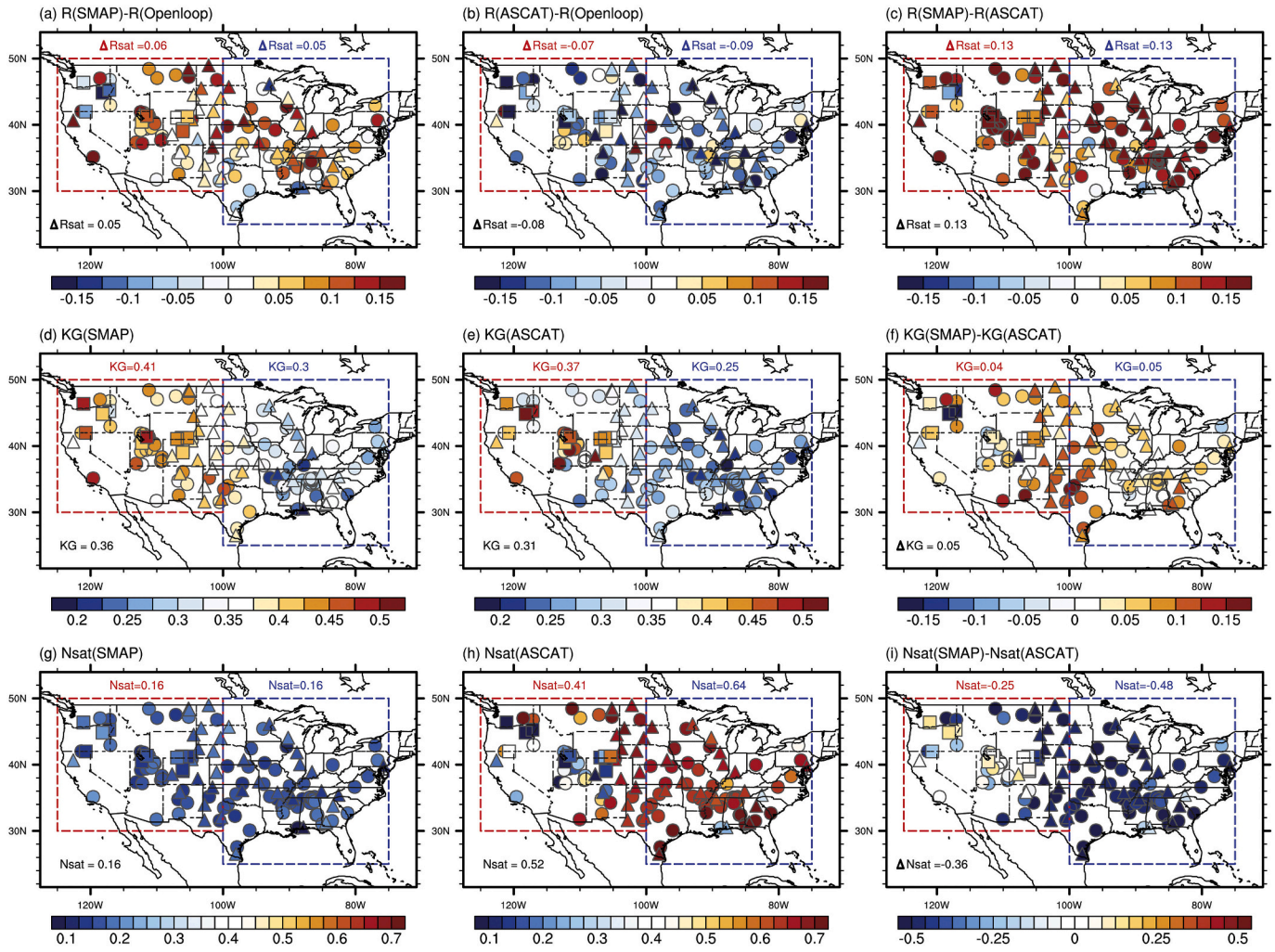

Fig. 6. The spatial distribution of (a, b) the skill difference between the satellite retrievals and the open loop (ΔR_{sat}), (d, e) the approximate Kalman gain (KG), and (g, h) the effective number of assimilated observational samples (N_{sat}). The results are from (a, d, and g) DA(SMAP) and (b, e, and h) DA(ASCAT). Panels (c, f, and i) in the last column show, separately for each row, the difference between the results for the two experiments. The bottom-left value in each panel represents the average across the entire domain. The red and blue dashed boxes indicate the western and eastern U.S., respectively, and the value above each box represents the average of the values within each box. The number of sites in the western and the eastern sub-domain is 69 and 66, respectively. (For interpretation of the references to colour in this figure legend, the reader is referred to the web version of this article.)

on the data source and the region. Fig. 5a and b show the spatial distributions of the skill improvement from the open loop by DA(SMAP) and DA(ASCAT) experiments, respectively. Both experiments generally show improved performance, especially in the western U.S., even though the skill increase is less pronounced in DA(ASCAT). The larger improvement in the western U.S. is consistent with the clear performance improvement over grasslands (i.e., Fig. 4), as most of the western U.S. is classified as grasslands. Fig. 5c compares the skill difference between DA(SMAP) and DA(ASCAT) (Fig. 5c). When the regions are separated into the western (125°W–100°W, 25°N–50°N) and the eastern U.S. (100°W–70°W, 25°N–50°N), the improvements from DA(SMAP) exceed those from DA(ASCAT) by $\Delta R \sim 0.06$ over the western U.S. and by $\Delta R \sim 0.03$ over the eastern U.S.. This result is further investigated in the following sub-section.

4.3. Component analysis for the skill improvement

In an effort to better understand the differences in the skill improvements among the soil moisture data assimilation experiments, this section examines the assimilation metrics introduced in Section 3.5. Specifically, this section further examines the following three key points: (i) the skill of DA(SMAP) is higher than DA(ASCAT), (ii) the two single-sensor assimilation experiments concurrently reveal the higher skill improvement in the western U.S. compared to the eastern U.S., and (iii) the skill difference in both single-sensor experiments is higher in the western U.S. compared to the eastern U.S..

Figs. 6 represents the spatial distributions of the assimilation metrics for the two single sensor assimilation experiments and their difference. The average ΔR_{sat} from SMAP is greater than that of ASCAT over the continental U.S. (Fig. 6a and b), mostly due to the higher skill of SMAP compared to ASCAT retrievals as indicated in Fig. 3d. The significantly better quality of the SMAP retrievals makes a clear difference in the results of the data assimilation (c.f., Fig. 5c).

Furthermore, KG values from the DA(SMAP) and DA(ASCAT) experiments are higher in the western than the eastern U.S. (Fig. 6d and e), which is mostly attributed to the spatial distribution of the model background error (E_b) rather than that of observation error (E_o) (not shown). Therefore, KG contributes to the improvement in the performance of data assimilation particularly in the western U.S. in both single-sensor assimilation experiments (c.f., Fig. 5a and b). Lastly, in trying to identify which factor plays a dominant role in the regional dependence of the skill improvement in the two single-sensor

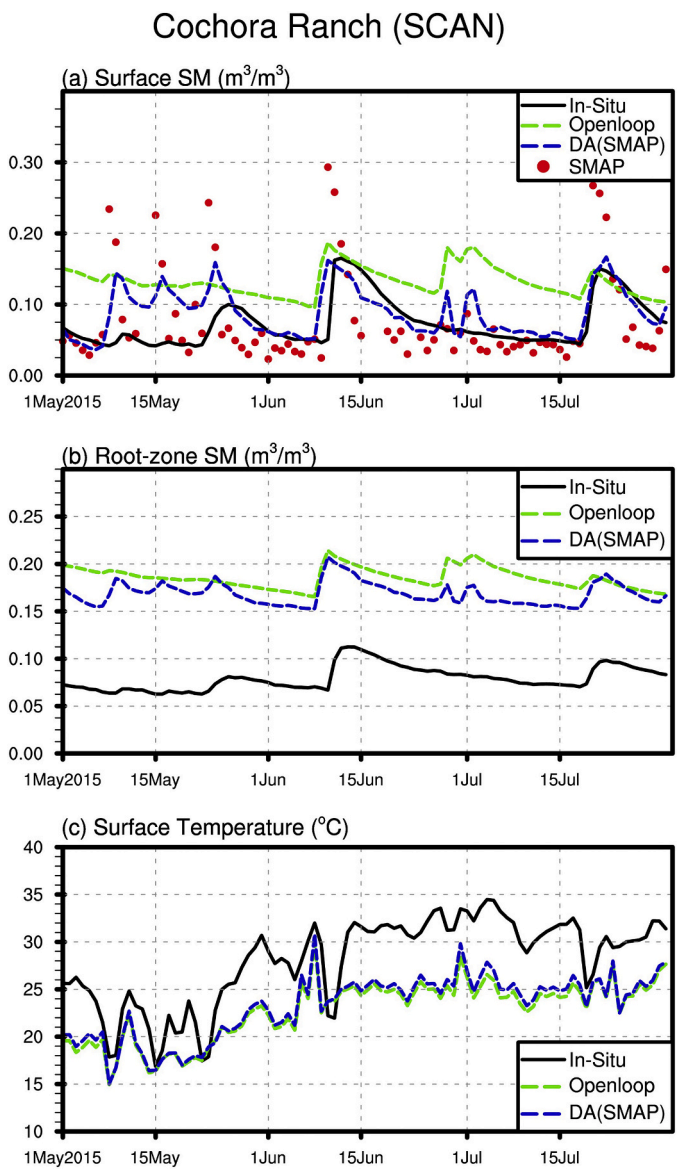

Fig. 7. Time series of (a) surface soil moisture, (b) root-zone soil moisture, and (c) land surface temperature at Cochora Ranch station (35.12°N, 119.6°W) in California from in situ measurements (black lines), DA(SMAP) (blue lines), the open loop model (green lines), and the SMAP retrievals (red dots). (For interpretation of the references to colour in this figure legend, the reader is referred to the web version of this article.)

experiments (Fig. 5c), we note that the ΔR_{sat} values for SMAP and ASCAT are similar for the western and eastern U.S. (Figs. 6c). This similarity for the western and eastern U.S. also applies to the *KG* difference values between DA(SMAP) and DA(ASCAT) (Fig. 6f). On the other hand, the corresponding N_{sat} difference values are quite different for the western and eastern U.S. (Fig. 6i). This west-east discrepancy primarily originates with the N_{sat} values for DA(ASCAT) (Fig. 6h) because there is little west-east discrepancy in DA(SMAP) (Fig. 6g).

Note also that the number of assimilated observations within each local patch is considerably smaller in DA(SMAP) than in DA(ASCAT) (compare Fig. 6g and h). For instance, the N_{sat} values for DA(SMAP) and DA(ASCAT) over the Continental U.S. are 0.16 and 0.52, respectively (Fig. 6g and h). First, ASCAT has finer spatial resolution than SMAP. Second, DA(ASCAT) utilizes two satellite sensors (METOP-A and METOP-B) in complementary orbits, instead of just one for DA(SMAP). Even accounting for the fact that ASCAT retrievals are from two satellite sensors (i.e., $N_{sat} = \sim 0.3$ for each of the two sensors), the ASCAT N_{sat} value is still nearly two times larger than that of SMAP, which can be explained by the difference in spatial resolution between SMAP and ASCAT. Additionally, the number of assimilated ASCAT observations in the eastern U.S. is larger than that in the western U.S., which is due to the quality control of the retrievals. For instance, ASCAT observations are discarded when the topographic complexity flag provided with the retrievals is larger than 10%. The mountainous terrain of the western U.S. thus leads to a decrease in N_{sat} for DA(ASCAT). When the quality control process for the ASCAT observations with topographic complexity is omitted in a separate, one-year (2016) experiment, the soil moisture assimilation skill drops by $\Delta R = -0.01$. Consequently, the skill values of the DA(SMAP) and DA(ASCAT) experiments are more different in the western U.S., because a relatively smaller number of ASCAT observations is assimilated there.

4.4. Validation of the drought event

There were several drought events since 2015 over the western U.S., especially in California. This section investigates the impact of soil moisture assimilation on the representation of hydrological climate extremes such as a severe drought. Hereafter the soil moisture estimates from DA(SMAP) are presented as the best performance results. Fig. 7 represents the daily time series of soil moisture and temperature from in situ observations, the open loop simulation, and DA(SMAP) at Cochora Ranch station in California during May–July 2015. DA(SMAP) clearly captures the dry surface and root-zone soil moisture conditions much better than the open loop simulation, even though the improvement is not always prominent due to the absence of satellite observations such as in mid-May when the SMAP retrieval is sampled much less. At this location, the RMSE of the surface (root-zone) soil moisture is reduced from 0.068 $m^3\ m^{-3}$ (0.107 $m^3\ m^{-3}$) for the open loop model to 0.035 $m^3\ m^{-3}$ (0.090 $m^3\ m^{-3}$) for the SMAP assimilation for May–July 2015. The drier soil moisture conditions in the assimilation experiment lead to the surface flux partitioning away from latent heat flux and toward increased sensible heat flux, which finally reduces the cold bias in the experiment. As a result, there is a slight improvement from the assimilation in the simulation of surface temperature.

Furthermore, the soil moisture assimilation estimates constrained by the SMAP satellite retrievals provide a more realistic spatial representation of drought conditions. The western U.S. suffered extreme drought from 2015 to 2016, with the most severe impacts seen in California (Supplementary Figs. 1 and 2, respectively). Fig. 8 represents the spatial patterns of the SMCI drought index based on surface soil moisture estimates. The figure shows that the spatial distribution of land surface dryness in the western U.S. is better represented by DA(SMAP) than in the open loop simulation. The drought index from the satellite assimilation for 2 years reveals more similar features to the U.S. drought monitoring information presented in the Supplementary Figures compared with the result of the open loop, especially in California, where the most severe drought occurred. The drought assessment only based on the assimilated soil moisture estimate shows the spatial distribution of the land surface dryness. In contrast, it is not consistent with the coherent dry conditions from the U.S. drought monitoring system based on various variables such as precipitation, surface temperature, streamflow, and so on, as well as soil moisture contents without any assimilation.

5. Conclusion

This study develops a data assimilation system based on the JULES land surface model and the LETKF scheme. The system assimilates soil moisture retrievals from L-band passive (SMAP) and C-band active (ASCAT) microwave remote sensing observations. The retrievals are subject to quality control and, prior to the data assimilation, are rescaled into the model soil moisture climatology using CDF fitting. Based on this

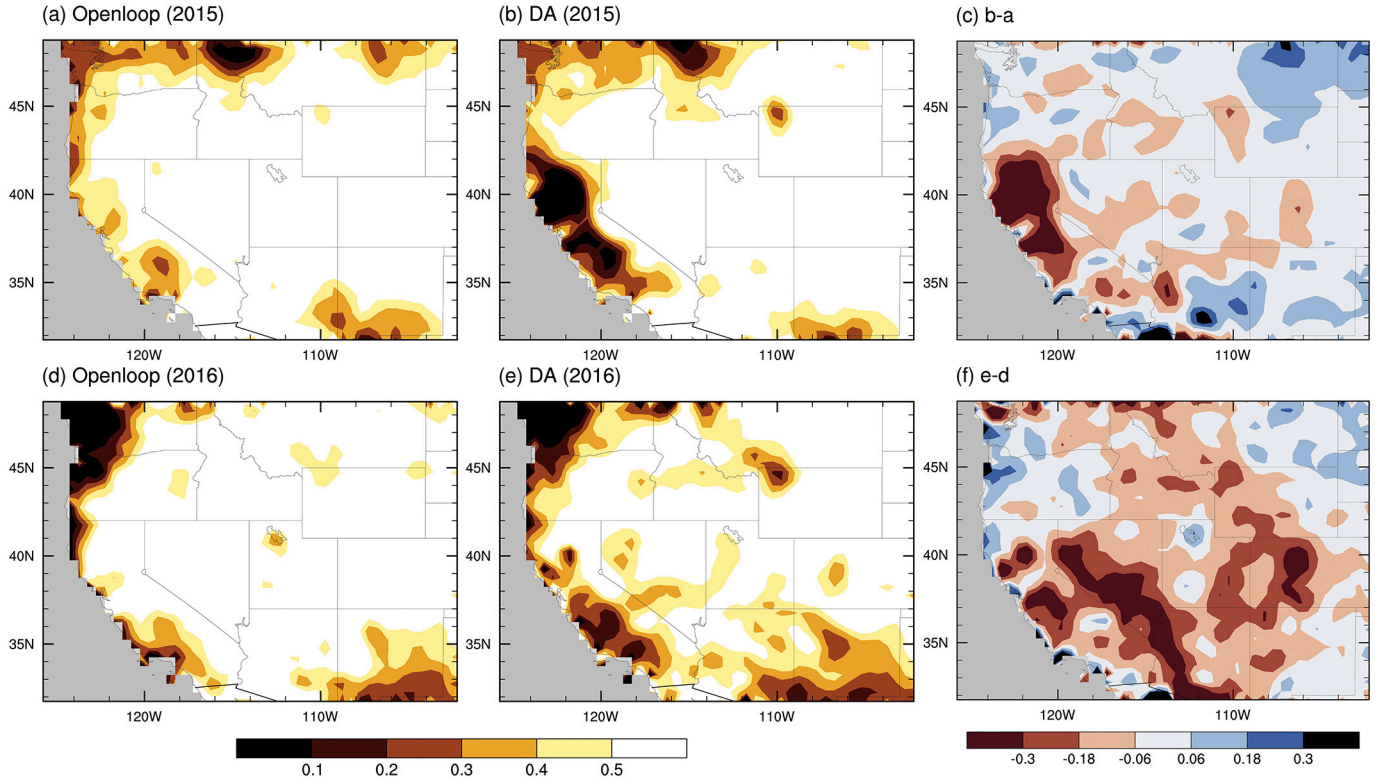

Fig. 8. Weekly SMCI drought index for 5 May–2 June 2015 (top row) and 3 May–31 May 2016 (bottom row) from the open loop model (left column) and DA(SMAP) (middle column). The SMCI difference between DA(SMAP) and the open loop is shown in the right column.

data assimilation framework, we examine the impact of remote sensing retrievals on the assimilated soil moisture estimates through validation with ground-based measurements. This study investigates three different soil moisture assimilation experiments with the LETKF scheme: (i) single-sensor assimilation of SMAP retrievals, (ii) single-sensor assimilation of ASCAT retrievals, and (iii) combined assimilation of SMAP and ASCAT retrievals. The results reveal that both sets of satellite retrievals provide added value in the representation of surface and root-zone soil moisture in the assimilation estimates over the continental U.S. The skill improvement is more pronounced in the relatively dry grasslands regions of the western U.S. The result from the SMAP assimilation experiment shows the best performance, with surface and root-zone soil moisture skill improvements of 0.05 and 0.03, respectively. On the other hand, the skill of the combined SMAP and ASCAT assimilation estimates is similar to that of the SMAP-only assimilation, suggesting that the assimilation of additional observations has little impact if they are of relatively lower quality.

The skill improvement of soil moisture estimates from the assimilation experiments can be broken into three different components. The three assimilation metrics are (i) the relative skill of satellite retrievals compared to that of the open loop, (ii) an approximation of the Kalman gain, and (iii) the number of assimilated observations. Based on this diagnostic, the skill of soil moisture estimates from the SMAP assimilation over the continental US is higher than that from the ASCAT assimilation mainly owing to the better quality of the SMAP retrievals. It is also found that the higher skill improvement in the western compared to the eastern U.S. is explained by the Kalman gain in both DA(SMAP) and DA(ASCAT). Moreover, the skill difference between two single-sensor assimilation experiments shows a large regional dependence. Specifically, the SMAP assimilation estimates show relatively higher skill compared to the ASCAT assimilation estimates in the western U.S. than in the eastern U.S.. This result is attributed mainly to the fact that relatively fewer ASCAT observations are assimilated in the western U.S.. During quality control, ASCAT retrievals are discarded when the topographical complexity index exceeds 10%. Even though there are smaller west-east differences in the relative skill of satellite retrievals and the Kalman gain between both experiments, the difference in the number of assimilated data contributes dominantly to the larger skill difference in the western U.S..

Finally, the assessment of drought conditions is enhanced through the assimilation of SMAP soil moisture retrievals. The soil moisture assimilation estimates better match the observed extremely dry conditions for the 2015 and 2016 western U.S. drought events. This finding corroborates the emerging use of SMAP soil moisture estimates in the U. S. Drought Monitor and suggests that soil moisture estimates from an advanced land data assimilation system that ingests SMAP and other satellite observations may further improve the current drought monitoring.

Looking further ahead, improved soil moisture estimates from the land data assimilation system developed in this study may also improve the initialization of dynamical forecast models. As the soil moisture strongly controls the energy and water balance at the land surface interface, this approach should lead to a better prediction of the atmospheric states through the realistic representation of land-atmosphere interaction. This is especially true in regions with scarce precipitation observations (e.g., much of South America, Africa, Asia, and Australia) where the performance of soil moisture estimates from open loop simulations is less reliable.

Declaration of competing interest

The authors declare that they have no known competing financial interests or personal relationships that could have appeared to influence the work reported in this paper.

Acknowledgments

This study was supported by the Korea Meteorological

Administration Research and Development Program under Grant KMI2018-03110. Rolf Reichle was supported by the NASA SMAP mission and the NASA SMAP Science Team.

Appendix A. Supplementary data

Supplementary data to this article can be found online at https://doi.org/10.1016/j.rse.2020.112222.

References

Albergel, C., De Rosnay, P., Gruhier, C., Muñoz-Sabater, J., Hasenauer, S., Isaksen, L., Kerr, Y., Wagner, W., 2012. Evaluation of remotely sensed and modelled soil moisture products using global ground-based in situ observations. Remote Sens. Environ. 118, 215–226.

Al-Yaari, A., Wigneron, J.-P., Dorigo, W., Colliander, A., Pellarin, T., Hahn, S., Mialon, A., Richaume, P., Fernandez-Moran, R., Fan, L., 2019. Assessment and inter-comparison of recently developed/reprocessed microwave satellite soil moisture products using ISMN ground-based measurements. Remote Sens. Environ. 224, 289–303.

Aonashi, K., Awaka, J., Hirose, M., Kozu, T., Kubota, T., Liu, G., Shige, S., Kida, S., Seto, S., Takahashi, N., 2009. GSMaP passive microwave precipitation retrieval algorithm: algorithm description and validation. J. Meteorol. Soc. Jpn. Ser. II 87, 119–136.

Bateni, S., Entekhabi, D., 2012. Relative efficiency of land surface energy balance components. Water Resour. Res. 48.

Bell, J.E., Palecki, M.A., Baker, C.B., Collins, W.G., Lawrimore, J.H., Leeper, R.D., Hall, M.E., Kochendorfer, J., Meyers, T.P., Wilson, T., 2013. US climate reference network soil moisture and temperature observations. J. Hydrometeorol. 14, 977–988.

Best, M., Pryor, M., Clark, D., Rooney, G., Essery, R., Ménard, C., Edwards, J., Hendry, M., Porson, A., Gedney, N., 2011. The Joint UK Land Environment Simulator (JULES), model description–Part 1: energy and water fluxes. Geosci. Model Dev. 4, 677–699.

Chan, S.K., Bindlish, R., O'Neill, P.E., Njoku, E., Jackson, T., Colliander, A., Chen, F., Burgin, M., Dunbar, S., Piepmeier, J., 2016. Assessment of the SMAP passive soil moisture product. IEEE Trans. Geosci. Remote Sens. 54, 4994–5007.

De Jeu, R.A., 2003. Retrieval of Land Surface Parameters Using Passive Microwave Remote Sensing. PhD diss.. Vrije Universiteit Amsterdam.

De Lannoy, G., Reichle, R., 2016. Assimilation of SMOS brightness temperatures or soil moisture retrievals into a land surface model. Hydrol. Earth Syst. Sci. 20, 4895–4911.

De Lannoy, G.J., Reichle, R.H., Houser, P.R., Arsenault, K.R., Verhoest, N.E., Pauwels, V. R., 2010. Satellite-scale snow water equivalent assimilation into a high-resolution land surface model. J. Hydrometeorol. 11, 352–369.

De Rosnay, P., Drusch, M., Vasiljevic, D., Balsamo, G., Albergel, C., Isaksen, L., 2013. A simplified Extended Kalman Filter for the global operational soil moisture analysis at ECMWF. Q. J. R. Meteorol. Soc. 139, 1199–1213.

Diamond, H.J., Karl, T.R., Palecki, M.A., Baker, C.B., Bell, J.E., Leeper, R.D., Easterling, D.R., Lawrimore, J.H., Meyers, T.P., Helfert, M.R., 2013. US Climate Reference Network after one decade of operations: status and assessment. Bull. Am. Meteorol. Soc. 94, 485–498.

Dirmeyer, P.A., Jin, Y., Singh, B., Yan, X., 2013. Trends in land–atmosphere interactions from CMIP5 simulations. J. Hydrometeorol. 14, 829–849.

Dobson, M.C., Ulaby, F.T., 1986. Active microwave soil moisture research. IEEE Trans. Geosci. Remote Sens. 23–36.

Dorigo, W.A., Scipal, K., Parinussa, R.M., Liu, Y.Y., Wagner, W., De Jeu, R.A.M., Naeimi, V., 2010. Error characterisation of global active and passive microwave soil moisture datasets. Hydrol. Earth Syst. Sci. 14 (12), 2605–2616. https://doi.org/10.5194/hessd-7-5621-2010.

Draper, C., Reichle, R., De Lannoy, G., Liu, Q., 2012. Assimilation of passive and active microwave soil moisture retrievals. Geophys. Res. Lett. 39.

Entekhabi, D., Njoku, E.G., O'Neill, P.E., Kellogg, K.H., Crow, W.T., Edelstein, W.N., Entin, J.K., Goodman, S.D., Jackson, T.J., Johnson, J., 2010a. The soil moisture active passive (SMAP) mission. Proc. IEEE 98, 704–716.

Entekhabi, D., Reichle, R.H., Koster, R.D., Crow, W.T., 2010b. Performance metrics for soil moisture retrievals and application requirements. J. Hydrometeorol. 11, 832–840.

Forman, B.A., Reichle, R., Rodell, M., 2012. Assimilation of terrestrial water storage from GRACE in a snow-dominated basin. Water Resour. Res. 48.

Friedl, M.A., Sulla-Menashe, D., Tan, B., Schneider, A., Ramankutty, N., Sibley, A., Huang, X., 2010. MODIS Collection 5 global land cover: algorithm refinements and characterization of new datasets. Remote Sens. Environ. 114, 168–182.

Gao, H., Wood, E.F., Jackson, T., Drusch, M., Bindlish, R., 2006. Using TRMM/TMI to retrieve surface soil moisture over the southern United States from 1998 to 2002. J. Hydrometeorol. 7, 23–38.

Hamill, T.M., Whitaker, J.S., Snyder, C., 2001. Distance-dependent filtering of background error covariance estimates in an ensemble Kalman filter. Mon. Weather Rev. 129, 2776–2790.

Houtekamer, P.L., Mitchell, H.L., 2001. A sequential ensemble Kalman filter for atmospheric data assimilation. Mon. Weather Rev. 129, 123–137.

Hunt, B.R., Kostelich, E.J., Szunyogh, I., 2007. Efficient data assimilation for spatiotemporal chaos: a local ensemble transform Kalman filter. Phys. D Nonlinear Phenom. 230, 112–126.

Kerr, Y.H., Waldteufel, P., Wigneron, J.-P., Delwart, S., Cabot, F., Boutin, J., Escorihuela, M.-J., Font, J., Reul, N., Gruhier, C., 2010. The SMOS mission: new tool for monitoring key elements ofthe global water cycle. Proc. IEEE 98, 666–687.

Kobayashi, S., Ota, Y., Harada, Y., Ebita, A., Moriya, M., Onoda, H., Onogi, K., Kamahori, H., Kobayashi, C., Endo, H., 2015. The JRA-55 reanalysis: general specifications and basic characteristics. J. Meteorol. Soc. Jpn. Ser. II 93, 5–48.

Koster, R., Mahanama, S., Yamada, T., Balsamo, G., Berg, A., Boisserie, M., Dirmeyer, P., Doblas-Reyes, F., Drewitt, G., Gordon, C., 2011. The second phase of the global land–atmosphere coupling experiment: soil moisture contributions to subseasonal forecast skill. J. Hydrometeorol. 12, 805–822.

Kubota, T., Shige, S., Hashizume, H., Aonashi, K., Takahashi, N., Seto, S., Hirose, M., Takayabu, Y.N., Ushio, T., Nakagawa, K., 2007. Global precipitation map using satellite-borne microwave radiometers by the GSMaP project: production and validation. IEEE Trans. Geosci. Remote Sens. 45, 2259–2275.

Lahoz, W.A., De Lannoy, G.J., 2014. Closing the gaps in our knowledge of the hydrological cycle over land: conceptual problems. Surv. Geophys. 35, 623–660.

Lievens, H., Reichle, R.H., Liu, Q., De Lannoy, G., Dunbar, R.S., Kim, S., Das, N.N., Cosh, M., Walker, J.P., Wagner, W., 2017. Joint Sentinel-1 and SMAP data assimilation to improve soil moisture estimates. Geophys. Res. Lett. 44, 6145–6153.

Liu, Q., Reichle, R.H., Bindlish, R., Cosh, M.H., Crow, W.T., de Jeu, R., De Lannoy, G.J., Huffman, G.J., Jackson, T.J., 2011. The contributions of precipitation and soil moisture observations to the skill of soil moisture estimates in a land data assimilation system. J. Hydrometeorol. 19.

Loveland, T.R., Belward, A., 1997. The IGBP-DIS global 1km land cover data set, DISCover: first results. Int. J. Remote Sens. 18, 3289–3295.

Miyoshi, T., Yamane, S., 2007. Local ensemble transform Kalman filtering with an AGCM at a T159/L48 resolution. Mon. Weather Rev. 135, 3841–3861.

Mladenova, I.E., Bolten, J.D., Crow, W.T., Sazib, N., Cosh, M.H., Tucker, C.J., Reynolds, C., 2019. Evaluating the operational application of SMAP for global agricultural drought monitoring. IEEE J. Sel. Top. Appl. Earth Obs. Remote Sens. 12, 3387–3397.

Owe, M., de Jeu, R., Walker, J., 2001. A methodology for surface soil moisture and vegetation optical depth retrieval using the microwave polarization difference index. IEEE Trans. Geosci. Remote Sens. 39, 1643–1654.

Owe, M., de Jeu, R., Holmes, T., 2008. Multisensor historical climatology of satellite-derived global land surface moisture. J. Geophys. Res. Earth Surf. 113.

Paloscia, S., Pampaloni, P., 1988. Microwave polarization index for monitoring vegetation growth. IEEE Trans. Geosci. Remote Sens. 26, 617–621.

Pan, M., Cai, X., Chaney, N.W., Entekhabi, D., Wood, E.F., 2016. An initial assessment of SMAP soil moisture retrievals using high-resolution model simulations and in situ observations. Geophys. Res. Lett. 43, 9662–9668.

Parinussa, R.M., Holmes, T.R., Wanders, N., Dorigo, W.A., de Jeu, R.A., 2015. A preliminary study toward consistent soil moisture from AMSR2. J. Hydrometeorol. 16, 932–947.

Reichle, R.H., 2008. Data assimilation methods in the Earth sciences. Adv. Water Resour. 31, 1411–1418.

Reichle, R.H., Koster, R.D., 2004. Bias reduction in short records of satellite soil moisture. Geophys. Res. Lett. 31.

Reichle, R.H., McLaughlin, D.B., Entekhabi, D., 2001. Variational data assimilation of microwave radiobrightness observations for land surface hydrology applications. IEEE Trans. Geosci. Remote Sens. 39, 1708–1718.

Reichle, R.H., McLaughlin, D.B., Entekhabi, D., 2002a. Hydrologic data assimilation with the ensemble Kalman filter. Mon. Weather Rev. 130, 103–114.

Reichle, R.H., Walker, J.P., Koster, R.D., Houser, P.R., 2002b. Extended versus ensemble Kalman filtering for land data assimilation. J. Hydrometeorol. 3, 728–740.

Reichle, R.H., Crow, W.T., Keppenne, C.L., 2008. An adaptive ensemble Kalman filter for soil moisture data assimilation. Water Resour. Res. 44.

Reichle, R.H., Kumar, S.V., Mahanama, S.P., Koster, R.D., Liu, Q., 2010. Assimilation of satellite-derived skin temperature observations into land surface models. J. Hydrometeorol. 11, 1103–1122.

Reichle, R.H., De Lannoy, G.J., Liu, Q., Ardizzone, J.V., Colliander, A., Conaty, A., Crow, W., Jackson, T.J., Jones, L.A., Kimball, J.S., 2017a. Assessment of the SMAP level-4 surface and root-zone soil moisture product using in situ measurements. J. Hydrometeorol. 18, 2621–2645.

Reichle, R.H., De Lannoy, G.J., Liu, Q., Koster, R.D., Kimball, J.S., Crow, W.T., Ardizzone, J.V., Chakraborty, P., Collins, D.W., Conaty, A.L., 2017b. Global assessment of the SMAP level-4 surface and root-zone soil moisture product using assimilation diagnostics. J. Hydrometeorol. 18, 3217–3237.

Reichle, R.H., Liu, Q., Koster, R.D., Crow, W.T., De Lannoy, G.J., Kimball, J.S., Ardizzone, J.V., Bosch, D., Colliander, A., Cosh, M., 2019. Version 4 of the SMAP level-4 soil moisture algorithm and data product. J. Adv. Model. Earth Syst. 11, 3106–3130.

Ridler, M.E., Madsen, H., Stisen, S., Bircher, S., Fensholt, R., 2014. Assimilation of SMOS-derived soil moisture in a fully integrated hydrological and soil-vegetation-atmosphere transfer model in W estern D enmark. Water Resour. Res. 50, 8962–8981.

Schaefer, G.L., Cosh, M.H., Jackson, T.J., 2007. The USDA natural resources conservation service soil climate analysis network (SCAN). J. Atmos. Ocean. Technol. 24, 2073–2077.

Schmugge, T., O'Neill, P.E., Wang, J.R., 1986. Passive microwave soil moisture research. IEEE Trans. Geosci. Remote Sens. 12–22.

Seneviratne, S.I., Lüthi, D., Litschi, M., Schär, C., 2006. Land–atmosphere coupling and climate change in Europe. Nature 443, 205–209.

Seneviratne, S.I., Corti, T., Davin, E.L., Hirschi, M., Jaeger, E.B., Lehner, I., Orlowsky, B., Teuling, A.J., 2010. Investigating soil moisture–climate interactions in a changing climate: a review. Earth Sci. Rev. 99, 125–161.

Seo, E., Lee, M.-I., Jeong, J.-H., Koster, R.D., Schubert, S.D., Kim, H.-M., Kim, D., Kang, H.-S., Kim, H.-K., MacLachlan, C., 2019. Impact of soil moisture initialization on boreal summer subseasonal forecasts: mid-latitude surface air temperature and heat wave events. Clim. Dyn. 52, 1695–1709.

Seo, E., Lee, M.-I., Schubert, S.D., Koster, R.D., Kang, H.-S., 2020. Investigation of the 2016 Eurasia heat wave as an event of the recent warming. Environ. Res. Lett. 15, 114018.

Sheffield, J., Goteti, G., Wood, E.F., 2006. Development of a 50-year high-resolution global dataset of meteorological forcings for land surface modeling. J. Clim. 19, 3088–3111.

Torres, R., Snoeij, P., Geudtner, D., Bibby, D., Davidson, M., Attema, E., Potin, P., Rommen, B., Floury, N., Brown, M., 2012. GMES Sentinel-1 mission. Remote Sens. Environ. 120, 9–24.

Ushio, T., Okamoto, K.i., Iguchi, T., Takahashi, N., Iwanami, K., Aonashi, K., Shige, S., Hashizume, H., Kubota, T., Inoue, T., 2003. The global satellite mapping of precipitation (GSMaP) project. Aqua (AMSR-E) 2004.

Ushio, T., Sasashige, K., Kubota, T., Shige, S., Okamoto, K.i., Aonashi, K., Inoue, T., Takahashi, N., Iguchi, T., Kachi, M., 2009. A Kalman filter approach to the Global Satellite Mapping of Precipitation (GSMaP) from combined passive microwave and infrared radiometric data. J. Meteorol. Soc. Jpn. Ser. II 87, 137–151.

Wagner, W., Hahn, S., Kidd, R., Melzer, T., Bartalis, Z., Hasenauer, S., Figa-Saldaña, J., de Rosnay, P., Jann, A., Schneider, S., 2013. The ASCAT soil moisture product: a review of its specifications, validation results, and emerging applications. Meteorol. Z. 22, 5–33.

Xu, L., Abbaszadeh, P., Moradkhani, H., Chen, N., Zhang, X., 2020. Continental drought monitoring using satellite soil moisture, data assimilation and an integrated drought index. Remote Sens. Environ. 250, 112028.

Yilmaz, M.T., Crow, W.T., 2013. The optimality of potential rescaling approaches in land data assimilation. J. Hydrometeorol. 14, 650–660.

Zhang, A., Jia, G., 2013. Monitoring meteorological drought in semiarid regions using multi-sensor microwave remote sensing data. Remote Sens. Environ. 134, 12–23.